Microvascular endowment in the developing chicken embryo lung

A. N. Makanya, R. Hlushchuk, O. Baum, N. Velinov, M. Ochs and V. Djonov

Am J Physiol Lung Cell Mol Physiol 292:L1136-L1146, 2007. First published 23 January 2007;
doi: 10.1152/ajplung.00371.2006

Am J Physiol Lung Cell Mol Physiol 292: L1136–L1146, 2007.
First published January 23, 2007; doi:10.1152/ajplung.00371.2006.

Microvascular endowment in the developing chicken embryo lung

A. N. Makanya,[1,2]* R. Hlushchuk,[2]* O. Baum,[2] N. Velinov,[2] M. Ochs,[2] and V. Djonov[2]

[1]*Department of Veterinary Anatomy and Physiology, University of Nairobi, Nairobi, Kenya; and* [2]*Institute of Anatomy, University of Bern, Bern, Switzerland*

Submitted 20 September 2006; accepted in final form 3 January 2007

Makanya AN, Hlushchuk R, Baum O, Velinov N, Ochs M, Djonov V. Microvascular endowment in the developing chicken embryo lung. *Am J Physiol Lung Cell Mol Physiol* 292: L1136–L1146, 2007. First published January 23, 2007; doi:10.1152/ajplung.00371.2006.—In the current study, the contribution of the major angiogenic mechanisms, sprouting and intussusception, to vascular development in the avian lung has been demonstrated. Sprouting guides the emerging vessels to form the primordial vascular plexus, which successively surrounds and encloses the parabronchi. Intussusceptive angiogenesis has an upsurge from embryonic *day 15* (E15) and contributes to the remarkably rapid expansion of the capillary plexus. Increased blood flow stimulates formation of pillars (the archetype of intussusception) in rows, their subsequent fusion and concomitant delineation of slender, solitary vascular entities from the disorganized meshwork, thus crafting the organ-specific angioarchitecture. Morphometric investigations revealed that sprouting is preponderant in the early period of development with a peak at E15 but is subsequently supplanted by intussusceptive angiogenesis by the time of hatching. Quantitative RT-PCR revealed that moderate levels of basic FGF (bFGF) and VEGF-A were maintained during the sprouting phase while PDGF-B remained minimal. All three factors were elevated during the intussusceptive phase. Immunohistoreactivity for VEGF was mainly in the epithelial cells, whereas bFGF was confined to the stromal compartment. Temporospatial interplay between sprouting and intussusceptive angiogenesis fabricates a unique vascular angioarchitecture that contributes to the establishment of a highly efficient gas exchange system characteristic of the avian lung.

sprouting angiogenesis; intussusceptive angiogenesis; vascular patterning; lung development; blood-gas barrier

LUNG DEVELOPMENT IN THE AVIAN species is a complex and little-studied process. The lung buds, which are the first signs of pulmonary development, arise from the floor of the primitive pharynx at ~3–4 days postincubation (8) in the chicken embryo of the domestic fowl (*Gallus gallus variant domesticus*). Whereas the pharyngeal endoderm gives rise to the bronchial tree, the mesenchyme forms the muscles, connective tissue, and the lymphatics that accompany the bronchial tree (8). In the avian embryo, the pulmonary and bronchial vasculature arises from the splanchnic plexus that forms around the foregut before the lung buds develop (19). In the chicken embryo, the pulmonary arteries are delineated at approximately embryonic *day 5* (E5) when the proximal part of the truncus arteriosus becomes incorporated into the right atrium, and the distal part is divided into the aorta and pulmonary artery by the aorticopulmonary septum (8). Generally, pulmonary vasculature arises by both vasculogenesis (18) and angiogenesis (30). Vasculogenesis starts with blood islands (18) that coalesce to form sinusoidal spaces of irregular profiles. Branches sprouting from the central pulmonary vascular trunks connect with the peripheral vascular channels establishing the primitive pulmonary vascular network (18). Furthermore, it has been shown that the peripheral pulmonary venous network develops earlier than the pulmonary arterial network (17). In the adult avian lung, the pulmonary arteries run alongside the airways, and the pulmonary veins show a similar branching pattern to the arteries, although separated from them. During early fetal development, the airways act as a template for pulmonary blood vessel development in that the vessels form by vasculogenesis around the branching airways (30).

Both vasculogenesis and sprouting angiogenesis (SA) are important players in the establishment of the pulmonary vasculature (see for example Refs. 5, 17, 18, 24, 39, 49). Indeed, embryonic mesodermal tissue contains angioblasts (43), which are capable of migration and initiation of vasculogenesis in the homing sites (3, 16). In adults, vasculogenesis occurs consequent to homing of circulating bone marrow-derived angioblasts (24).

In the avian lung, vasculogenesis has been reported by Maina (39) and Anderson-Berry et al. (5). Development of the vasculature in the avian lung results in an elaborate pattern of supplying and draining vessels that culminates in the dense cylindrically arranged capillary networks associated with the parabronchi, the ultimate sites of robust gas exchange in the avian lung (50). The chronological events, processes, and mechanisms as well as the molecules that lead to this pattern are, however, unknown. In the avian kidney, we have recently shown that sprouting precedes intussusceptive angiogenesis (IA) but the latter process participates in the ultimate multiplication and remodeling of vascular branches (41).

IA, a novel mechanism of vascular growth, expansion, and remodeling, has received impetus in the recent past, with the indication that it proceeds faster and at lower energetic costs than SA and preserves physiological status since extensive cell proliferation and basal membrane degradation are not required (11, 20). The quintessence of IA is transvascular pillar formation, and the mechanism comprises three cognates expressed in sequential, albeit overlapping, chronological phases (20, 21). Intussusceptive microvascular growth is the first process, which greatly expands the vascular network; intussusceptive arborization delineates the classic vascular tree pattern; and intussusceptive branching remodeling modifies the vascular pattern in regard to the physiological requirements (20). In the current study, we have systematically followed the development of the pulmonary vasculature from the formative embryonic stages to the time of hatching. SA plays an important role

* A. N. Makanya and R. Hlushchuk contributed equally to this study.

Address for reprint requests and other correspondence: V. Djonov, Institute of Anatomy, Univ. of Bern, Balzerstrasse 2, 3000 Bern, Switzerland (e-mail: djonov@ana.unibe.ch).

The costs of publication of this article were defrayed in part by the payment of page charges. The article must therefore be hereby marked "*advertisement*" in accordance with 18 U.S.C. Section 1734 solely to indicate this fact.

Table 1. *Oligonucleotide sequences used in PCR reactions*

Number	Gene	Sense Primer	Antisense Primer	Length
NM_205433	basic FGF	5′-ggcactgaaatgtgcaacag-3′	5′-tccaggtccagtttttggtc-3′	151
AB031025	PDGF-B	5′-cttgaacccggcatgaat-3′	5′-ctatgctatgaggatttctttcagc-3′	735
AB011078	VEGF-A	5′-atgaactttctgctcacttgg-3′	5′-ccgtctcggtttttcacatc-3′	648
NM_205518	β-actin	5′-ccagccatctttcttgggta-3′	5′-agtcaagcgccaaaagaaaa-3′	455

in the basic pattern establishment, whereas the culmination of great expansion and maturation of the vasculature is by IA.

MATERIALS AND METHODS

Experimental animals. Brown Leghorn eggs were incubated at 37°C and a humidity of 65%. Embryos covering Hamburger and Hamilton stages 19 to 45, which correspond to E3 to E21 of incubation, were obtained and processed according to the methods described below. In addition, adult Rhode Island Red layers (*Gallus gallus variant domesticus*) already identified for culling were killed with intra-abdominal injection of Euthatal (sodium pentobarbitone). All protocols were approved by the Animal Care and Use Committee of the University of Nairobi.

Intravascular methylmethacrylate casting. Embryos were perfused with a solution of 0.9% sodium chloride containing 1% liqemin and 1% procaine through the vitelline artery, whereas the adult birds were perfused through the heart. The vasculature was then filled with methylmethacrylate resin (Mercox; Vilene Hospital, Tokyo, Japan) containing 0.1 ml of accelerator per every 5 ml of the resin. One hour after perfusion, either the entire embryo or specific targeted organs were immersed in Ringer solution for at least 2 h and subsequently transferred to a 15% potassium hydroxide solution for 2–4 wk. After dissolution of the tissues, the casts were washed with water, dehydrated in ascending concentrations of ethanol, and dried in a desiccator. Samples were mounted on aluminium stabs, sputter-coated with gold, and viewed under a Philips XL 30 FEG scanning electron microscope.

Intratracheal methylmethacrylate casting. To assess the development of the bronchial network, methylmethacrylate was injected directly into the trachea and allowed to set, and the respiratory system was dissected out. The soft tissue was then digested as detailed above, and the casts were viewed by stereomicroscopy, and, in addition, sputter-coated with gold and viewed under a Philips XL 30 FEG scanning electron microscope.

Double methylmethacrylate casting. To study the interaction between the developing airways and the gas exchange system with the formative vasculature, a double casting system was employed. This first entailed performing intravascular casting with red-colored Mercox as outlined above followed by intratracheal infusion of blue Mercox. Samples were viewed by stereomicroscopy, and, in addition, under a scanning electron microscope as described above.

Light and electron microscopy. For both light microscopy and electron microscopic studies, embryos were fixed using a solution of 2.5% glutaraldehyde in 0.1 M cacodylate buffer (pH 7.4, 350 mosmol/kgH_2O). Embryos below 5 days of incubation were fixed by total immersion in the fixative while the rest were fixed by perfusion through vitelline vessels. Lungs were dissected out and diced into small blocks. Tissue blocks were postfixed in osmium tetroxide, block stained using

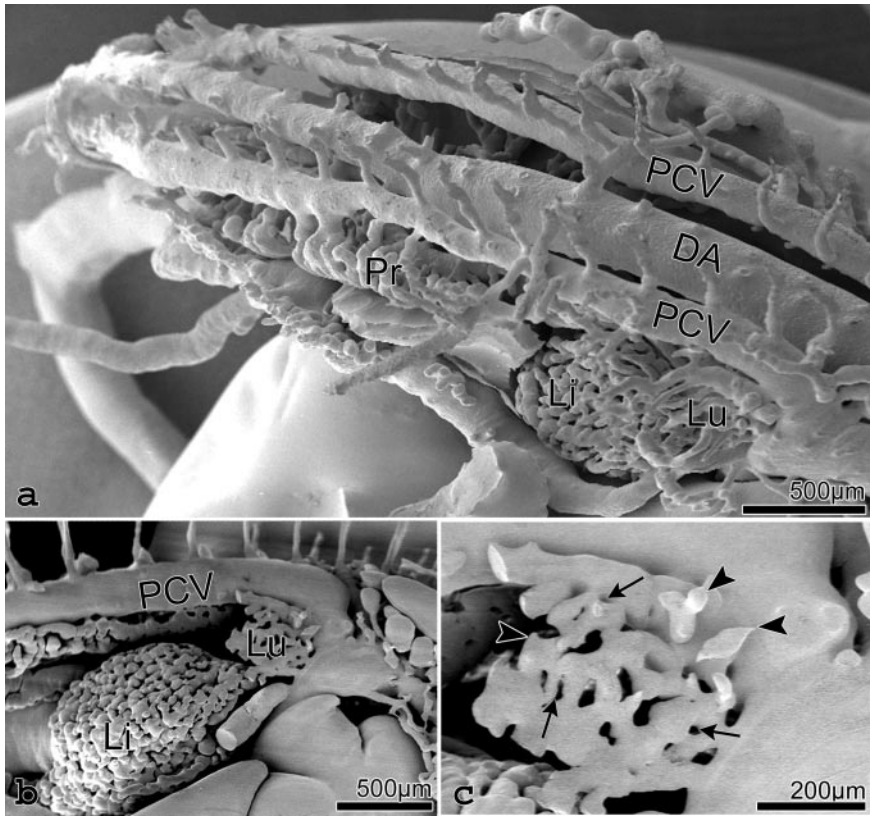

Fig. 1. Corrosion casts from developmental *day 5* (E5) demonstrating the developing avian pulmonary vasculature. *A*: at early E5, the lung vasculature comprises only a few sprouting blood vessels that form a rather simple pulmonary plexus (Lu), which is located cranial to and is continuous with the hepatic one (Li). The vascular plexus of the pronephros (Pr) is located in the caudal part of the embryo ventral to the major vessels. PCV, posterior cardinal vein; DA, dorsal aorta. *B*: the Lu later at E5 appears more complex. The vessels have a generally thicker girth and irregular shapes. The Li is also better developed. *C*: the pulmonary plexus expands by sprouting (arrowheads) and intussusceptive angiogenesis. The latter process is represented by tiny holes in the more central parts of the plexus (arrows). *C* is an inset of *B* at higher magnification.

uranyl acetate, dehydrated through ascending concentrations of ethanol, and embedded in epoxy resin. Semithin sections were obtained at a nominal thickness of 1 μm, stained with toluidine blue, and viewed under a Vanox BHS light microscope or Coolscope Digital Microscope (Nikon). Ultrathin sections were obtained at 90 nm, counterstained with lead citrate, and viewed on a Philips EM-300 microscope.

Morphometry of the pulmonary vascular casts. Intravascular Mercox casts of the chicken embryo lungs were taken at selected developmental days between E10 and E20. Three pulmonary casts per each age group were used. All morphometric measurements were done on the lateral surfaces of the pulmonary vascular casts where the blood vessels were unambiguously identifiable. The specimens were observed using a Philips XL 30 FEG scanning electron microscope. A test system of 96 points was superimposed on a computer monitor connected to the scanning electron microscope. Profiles of the vascular casts were displayed directly on the monitor screen, and areas of profiles were estimated directly by point counting. For each specimen, at least five randomly chosen positions were used for quantification of vessel area density, sprout, and pillar numerical densities. Pillars were identified as holes in vascular casts with diameters roughly measured less or equal to 2.5 μm. All holes greater than 2.5 μm normally referred to as meshes were ignored. Capillary sprouts were identified as tapered blind ending capillary branches.

Vessel area density. Vessel area density [A_A(Vs)] was obtained as the ratio of total number of points falling on vascular cast surfaces [Pp(Vs)] to the total number of points falling on the study area [Pp(ref)]. Thus $A_A(Vs) = Pp(Vs)/Pp(ref)$, where Pp(Vs) is the total number of points falling on vessel profiles, and Pp(ref) is the total number of points in the entire reference area.

Numerical density of the pillars. Numerical density of the pillars [NA(Pr)] is the total number of pillars counted per mm^2 of study area. Counting frames with a forbidden line (27a) was established so that the number of pillars per unit area could then be computed.

Relative numerical density of the pillars. Relative numerical density of the pillars [N_A(Pr,Vs)] is the total number of pillars counted per mm^2 of vessel area. This was estimated as a product of numerical density of the pillars and the vessel area density. Thus $N_A(Pr,Vs) = N_A(Pr) \times A_A(Vs)$.

Numerical density of the sprouts. Numerical density of the sprouts [N_A(Spr)] is the total number of sprouts counted per mm^2 of study area. Counting frames were established as described above, and the number of pillars per unit area was computed.

Relative numerical density of the sprouts. Relative numerical density of the sprouts [N_A(Spr,Vs)] is the total number of sprouts counted per mm^2 of vessel area. This was obtained as a product of the numerical density of sprouts and the vessel area density. Thus $N_A(Spr,Vs) = N_A(Spr) \times A_A(Vs)$.

Quantitative real-time RT-PCR. Total mRNA was prepared from chicken embryo lungs ($n = 3$) on E8, E11, E13, E15, E17, E18, E19 and E20 using the RNeasy Protect Mini kit (Qiagen, Basel, Switzerland) according to the manufacturer's protocol. Finally, the concentrations of the mRNA obtained were photometrically determined. cDNA was synthesized by RT with 2 mg of total RNA using 1 μM oligo(dT) primers and 4 units of Omniscript reverse transcriptase (Qiagen) at 37°C for 1 h according to the manufacturer's protocol. The cDNA samples were analyzed by quantitative PCR using pairs of primers specific for each of the genes (see Table 1).

For each sample, 200 ng of cDNA template were added to 12.5 μl of QuantiTect SyBR green master mix (Qiagen) and 0.15 μl of both sense and antisense primers (final concentration of 0.6 μM each) were added to a total volume of 20 μl with RNA-free water. An initial denaturing step at 95°C for 15 min was followed by 40 cycles with a

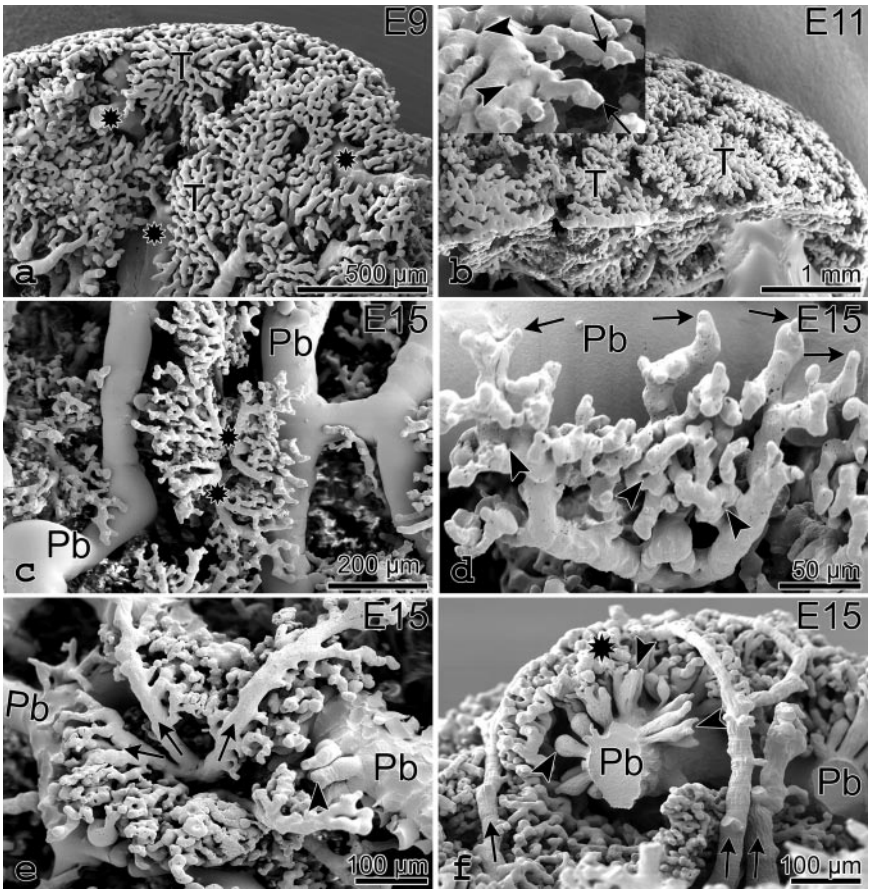

Fig. 2. Corrosion casts from the avian lung vasculature (*A* and *B*) and double-injection Mercox casts (*C–F*) illustrating the developing pulmonary microvasculature and its relationship to the parabronchial system. *A* and *B*: at E9 and E11, the pulmonary vasculature is organized into tree-like capillary tufts (T) comprising major supplying vessels [formative interparabronchial and parabronchial arteries (*) connected to capillary plexuses]. Vacant spaces between the tufts represent the areas occupied by the parabronchial system. The capillaries at the periphery of the tufts (*B*) expand predominantly by sprouting (arrows), whereas the central part grows by intussusception (arrowheads). Inset: part of *B* at higher magnification. *C* and *D*: double-injection Mercox casts showing the spatial relation between the developing lung vasculature and the parabronchi (Pb) at E15. The parabronchial arteries (*) give rise to the arterioles that form the dense network of capillaries that surround the Pb. The capillary network expands predominantly by sprouting (arrows) in peripheral parts of the tufts, followed by intussusceptive pillar formation (arrowheads in *D*). *D* is an *inset* of *C*. *E* and *F*: several arterioles (arrows) emerge from a common parabronchial artery and course towards opposite sides to supply adjacent Pb and the atria with incipient infundibula and air capillaries (arrowheads). The parabronchial arteries (arrows) supply the plexus from the outside while the veins send branches to the inside (not shown, see Fig. 4 for details).

denaturating step at 94°C (15 s), an annealing step at 56°C (30 s), and an elongation step at 72°C (60 s). For analysis, cycling reports and melting curves were evaluated. All the reactions were done in triplicate.

Immunohistochemistry. Specimens for immunohistochemical evaluation of VEGF and basic FGF (bFGF) were processed according to Makanya et al. (41) from embryos covering stages 25 to 45 (E4.5 to E20). Briefly, at least three specimens per time point were fixed in 2% paraformaldehyde and embedded in paraffin wax. Sections were dewaxed in xylene, rehydrated in ethanol, and rinsed in Tris-buffered saline (TBS: 50 mM Tris·HCl, pH 7.4, containing 100 mM sodium chloride). Before incubation with antibodies, the sections were put in a microwave oven (180 W) for 15 min. After blocking of unspecific binding in TBS containing 1% casein (Sigma 8654) for 10 min, the sections were incubated with the first antibody diluted in TBS: rabbit anti-VEGF, diluted 1:200 in TBS (sc-152; Santa Cruz Biotechnology, Santa Cruz, CA), or mouse anti-bFGF, diluted 1:150 in TBS (Upstate Biotechnology, Ab-05-118) for 15 h at 48°C. Subsequently, the sections were exposed to an affinity-purified biotinylated second antibody (anti-mouse EO 433, anti-rabbit EO 353; Dako, Glostrup, Denmark, diluted 1:200 in TBS) for 45 min at ambient temperature, washed three times in TBS, and then treated with the avidin-biotin-complex/horseradish peroxidase (P355, Dako) for a similar period at the same temperature. The reaction product was visualized by exposing sections to 3-amino-9-ethylcarbazole or 3,3-diaminobenzidine (Sigma Chemical, St. Louis, MO), which were then mounted in Aquatex (Merck, Darmstadt, Germany). Negative controls were performed using nonspecific mouse and rabbit sera.

RESULTS

At E5 (stage 27), a simple pulmonary plexus represented the developing lung. This plexus (Fig. 1*A*) was made up of a few

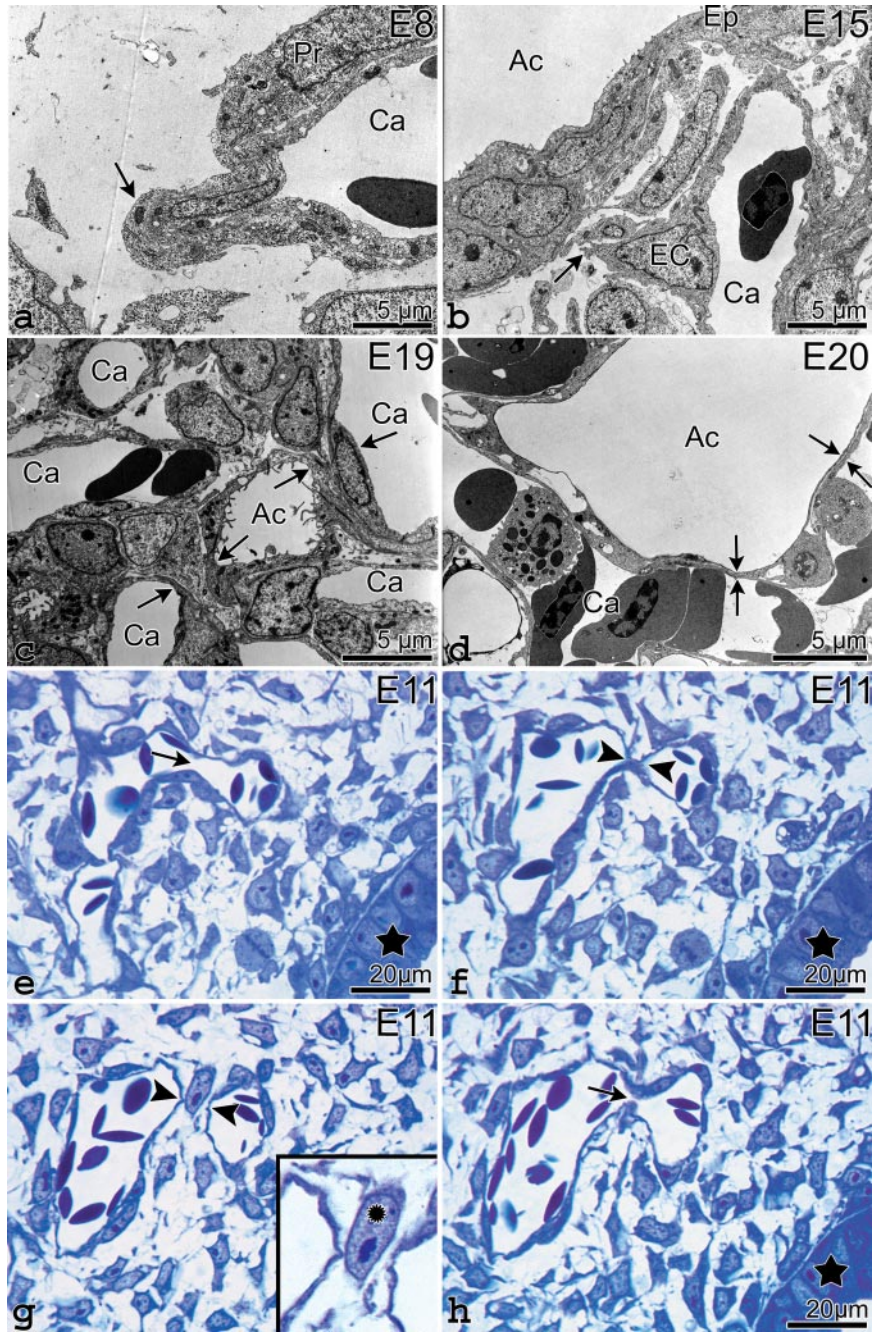

Fig. 3. Transmission electron microscopy micrographs demonstrate sprouts, morphological phenotypes (*A* and *B*), and formation of the blood-gas barrier (*C* and *D*). Light microscopy micrographs (*E–H*) illustrate a pillar, the archetype of intussusceptive angiogenesis. *A*: an early blood capillary sprout at E8 with a tapering migrating end (arrow) and slit-like lumen. Notice the absence of basal membrane and rarefied extracellular matrix surrounding the tip of the sprout. *B*: a sprout (arrow) originating from a polarized endothelial cell (EC) of a blood capillary (Ca) approaching the epithelium (Ep) of an air capillary (Ac) at E15. *C*: at E19, the blood capillaries approach the developing air capillaries to establish the blood-gas barrier (double arrows), which at this time is relatively thick. *D*: dramatic attenuation of the air capillary epithelium and reduction of the interstitial tissue results in a remarkably thin blood-gas barrier (double arrows) by E20. *E–H*: serial semithin sections showing the extents of a transluminal pillar in a lung capillary at E11. The open lumen of the vessel in *E* (arrow) is closed by a transluminal pillar in *F* and *G* (double arrowheads) and becomes open again at the end of the pillar (arrow in *H*). The parabronchial epithelium (stars) is used as a landmark to show that this is the same vessel. A pericyte (*inset* in *G*) is typically associated with the transluminal tissue pillar. The step section was 3 μm.

blood vessels situated close to the more endowed hepatic plexus, an analogy, which underpins the common origin of the two organs from the primitive gut. The lung was topographically cranial to the liver, and its vasculature was also continuous with that of the posterior cardinal vein and also the dorsal aorta. A few hours later (later at E5), the pulmonary plexus became more complex (Fig. 1, *B* and *C*), the vessels having a generally thicker girth and irregular shapes. At this stage, capillary sprouts were visible, particularly in the periphery, as well as sparse holes in the most central regions (representing transluminal tissue pillars, the quintessence of IA).

The pattern of pulmonary vasculature by E9 (stage 33, Fig. 2) was well organized into tree-like capillary tufts comprising a major supplying vessel with filial branches from which the capillary sprouts emanated. Empty spaces between the tufts (Fig. 2, *A* and *B*) marked the areas occupied by the developing airway system and gas exchange channels. At this stage, SA (Fig. 2*B*) appeared to supplant pillar formation so that the few tiny holes evident remained shallow and narrow at the expense of numerous robust sprouts. The pillars remained few and were restricted to the expanded areas of the capillaries.

The extent and intensity of centrifugally sprouting became augmented so that at E15 capillary sprouts from contiguous tufts approximated each other and started to anastomose, and by doing so enclosed the developing parabronchi (Fig. 2, *C–F*). From the aforementioned capillary tufts, larger supplying vessels (arterioles) were delineated (Fig. 2, *C–F*), and these appeared to develop above the general capillary network. These arterioles then approximated each other at the level of the middle long axes of the parabronchus and started to anastomose (Fig. 2, *E* and *F*). At the same time, the capillary plexus was augmented by massive SA with only sparse pillar holes being apparent.

Double Mercox casting (intratracheal and intravascular) demonstrated the relationship between the developing vasculature and parabronchi (Fig. 2, *C–F*). At the ventro-posterior part of the lung, the secondary bronchi gave rise to the branching neopulmonic parabronchi (not shown), and the tree-like capillary tufts grew between the parabronchi (Fig. 2*C*). The formative atria were evident on the surface of the parabronchi and appeared as rounded mounds of cast protruding from the parabronchus (Fig. 2, *E* and *F*). The development of the blood vessels was deftly harmonized with that of the gas exchange system so that as the blood capillary network was forming, the atria as well as the infundibula and air capillaries started to form (Fig. 2, *E* and *F*).

The prolonged sprouting phase of the pulmonary vasculature development presented a host of sprout morphophenotypes. As indicated in Fig. 3, the capillary sprouts showed morphological polarization of the endothelial cells with abluminal protrusions. The cell membrane at the tip of the sprout appeared amorphous, and the area surrounding the sprouts (sprout mantle) was rather rarefied. Furthermore, such cells had abundant cytoplasm and organelles, and the basement membranes were often absent (Fig. 3, *A* and *B*). The sprouts grew around the developing air conduits and at same time approximated the air capillaries (Fig. 3*B*). Microvessel apposition to the air capillaries led to progressive attenuation of the blood gas barrier so that by the time of hatching, a thin squamous epithelium was formed (Fig. 3, *C* and *D*).

Transluminal tissue pillars, the classic paradigm of IA, were captured in serial semithin sections (Fig. 3, *E–H*). These pillars correspond to the tiny holes observable in the vascular casts. A periendothelial cell (pericyte or smooth muscle cell) is typically trapped within the transluminal tissue pillar (Fig. 3*G*).

During formation of the parabronchial vascular plexus at E17 (Fig. 4), arterioles emanating from the parabronchial arteries migrated across the external aspect of the parabronchial capillary plexus and elongated to anastomose with those from the opposite side at the level of the long axis of the parabronchus. Additional lateral arteriolar branches formed and gave rise to the parabronchial capillary plexus. The primary parabronchial arterioles constricted in the plane of the long axis and were then broken into capillaries, probably by the process of pillar formation (Fig. 4*B*). The parabronchial plexus was drained by large interparabronchial veins, which were connected to the internal aspect of the parabronchial capillary plexus by short venules (Fig. 4, *C* and *D*). The well-developed

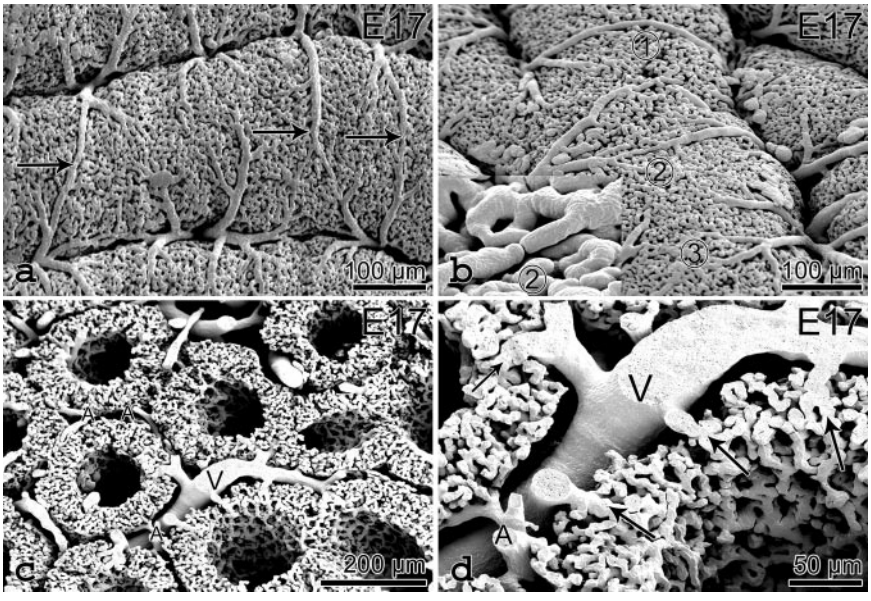

Fig. 4. External view (*A* and *B*) and cross section (*C* and *D*) through corrosion casts from E17 chicken lung demonstrating the developing supplying vasculature in the parabronchial unit. *A*: arteriole arcades (arrows) emanating from the parabronchial arteries ramify on the external aspect of the parabronchial capillary plexus. *B*: with the formation of lateral branches, the anastomosed arterioles break into capillaries: the initially continuous vessels (*region 1*) become constricted and discontinuous (*region 2*) and then retract giving way to the capillary plexus (*region 3*). The *inset* is part of *region 2* at higher magnification. *C* and *D*: the venous system is represented by large draining interparabronchial veins (V) connected to the inner aspect of the parabronchial capillary plexus by short venular branches (arrows). In contrast, the parabronchial arterioles (A) join the outer plexus site. *D* is an *inset* of *C* at higher magnification. The vessel indicated by V is a vein. The branches originating from this vein pierce through the capillary plexus but are short because of the early developmental stage. Later, they develop to well-ramified veins at the inner aspect of the Pb vasculature.

arterial vascular tree supplied the outer aspect of the parabronchial plexus via a multitude of parabronchial arterioles (Fig. 4, *C* and *D*).

At E20, arcuate arterioles surrounding the parabronchi were broken down so that no more direct anastomoses between arterioles in the external aspect were encountered (Fig. 5*A*). An overview of the parabronchial vascular plexuses revealed the elaborate topographical disposition of the interparabronchial arteries and veins. Venular branches from the vein pierced through the parabronchial capillary plexus and then broke into several capillaries that ramified hierarchically in the internal aspect of the parabronchial capillary plexus. In contrast, the arteriolar branches from the interparabronchial arteries broke into superficial arterioles whose capillary branches inosculated the general parabronchial plexus (Fig. 5, *A* and *B*).

In the formative stage, the parabronchial capillary plexus was a jumbled mass with holes representing the atria (Fig. 4, *C* and *D*). However, the process of intussusceptive arborization rapidly remodeled the meshwork in three steps, which could be summarized as follows. At the beginning, tissue pillars arose in rows, reshaped and fused hence delineating small collecting venules around the atria from the internal aspect of the parabronchial plexus (Fig. 5, *C* and *D*). In the subsequent step, segregation of individual atrio-infundibular vascular units by transluminal folds occurred, which severed the vascular bridges between the atria (Fig. 5, D and *E*). Consequent to this process, the blood flow direction was reoriented to be orthogonal to the long axis of the air capillaries, thus establishing the cross-current exchange system characteristic of the avian lung. Notably, the aforementioned rearrangement resulted in blood flowing directly from the arteries to the veins, continuous capillaries rather than the disorganized meshwork. This resulted from rearrangement of pillars in rows resembling a "necklace" pattern. Subsequent pillar elongation and fusion delineated straight solitary segments around the atria (Fig. 5, *F–H*, see also Fig. 6). In the adult chicken, pillars were observed only occasionally, unlike the situation before, and the capillaries were uniform, slender, and less branched (Fig. 6).

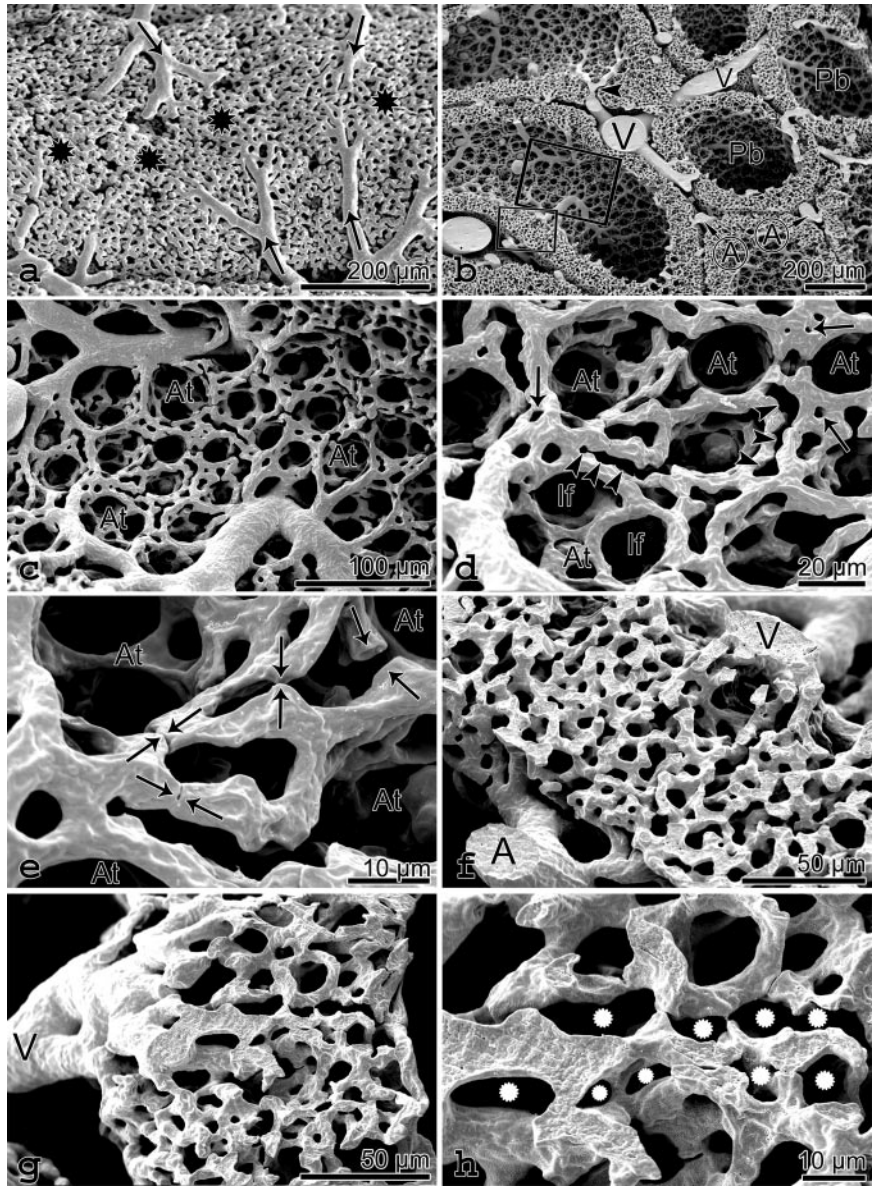

Fig. 5. External view (*A*) and cross sections (*B–H*) through the vascular corrosion casts from E20 chicken lung demonstrating the developing parabronchial vasculature. *A*: the parabronchial arterioles (arrows) split hierarchically into smaller branches that connect to the capillary plexus (*). No more direct anastomoses between arterioles are encountered. *B*: an overview of the parabronchial vascular plexuses showing the topographical disposition of the interparabronchial arteries (A) and veins (V). Venular branches (arrowheads) from the interparabronchial veins pierce through the parabronchial capillary plexus and then successively ramify on the internal surface of the parabronchial capillary plexus. Pb, parabronchial lumen. *C–E*: internal view of the parabronchial vasculature demonstrating the segregation of the atrial microvasculature. The capillary plexus is organized into an irregular meshwork surrounding the atria (At). The meshwork expands by insertion and enlargement of a multitude of tissue pillars (arrows in *D*). Many of the pillars reshape and fuse progressively (arrowheads in *D*) delineating straight solitary segments around the atria (At) and infundibula (If) from the chaotic capillary meshwork. Vascular connections between the atria are severed by transluminal folds (double arrows in *E*) and retraction, which results in segregation of individual atrio-infundibular vascular units. *C* is an *inset* of *B* (see larger rectangle in *B*), *D* is an *inset* of *C*, and *E* is an *inset* of *D*. *F–H*: cross section through vascular casts of the parabronchial capillary plexus showing the delineation of the gas exchanging capillaries. The capillary meshwork between the arteriole (A) and the venule (V) is initially irregular with randomly distributed pillars. Subsequently, the pillars rearrange in rows resembling a "necklace" pattern between the arterioles and venules (*F* and *G*). Pillar elongation and fusion in this axis (* in *H*) delineates solitary capillary segments surrounding the atria and air capillaries. *H* is an *inset* of *G*.

The knowledge about the quantitative aspects of the interplay between the sprouting and intussusceptive morphogenetic events elucidated their temporospatial involvement. The contribution of sprouting and intussusceptive modes of angiogenesis was captured by morphometry and is depicted in Fig. 7 and summarized schematically in Fig. 8. Vessel area density was highest at ~E17 (Fig. 7*A*), and this was mainly as a result of sprouting coupled with IA. The two mechanisms drove vascular development hand in hand. Sprouting was predominant during the early phase of lung development, with a dramatic peak at E17, and declined steadily towards E20. Sprouting was responsible for the formation of the basic vascular pattern. Subsequently, IA supplanted this process and was responsible for the rapid expansion of the lung microvasculature and formation of the final vascular pattern, which is functionally adequate and guarantees optimal gas exchange.

Real-time RT-PCR (Fig. 9) demonstrated a specific cDNA expression pattern for PDGF-B, bFGF, and VEGF. VEGF and bFGF gene expression remained at relatively constant levels up to E15, when both started to increase, with a peak at E17. Henceforth, bFGF expression declined and remained at lower levels, whereas VEGF only showed a slight decline followed by an additional steady rise from E19 onward. PDGF-B gene had a moderate expression in the early days of angiogenesis (up to E11), and then it distinctly declined between E11 and E15 and then increased dramatically at E19 to drop down to the initial position in 24 h. The immunoreactivity for VEGF and bFGF are summarized in Fig. 9. VEGF was strongly expressed in the lung epithelial cells and less in the stroma. On the contrary, bFGF was diffusely expressed in the stromal compartment and small feeding vessels.

DISCUSSION

Although recent studies have investigated pulmonary development in the avian species (36–40), only a few recent reports have made substantial reference to the developing vasculature (5, 39). The developmental process in the avian pulmonary vasculature results in a rather unique pattern of vessels surrounding the parabronchi and a dexteriously crafted blood capillary network that interlaces with the equally complex air capillary labyrinth (34). This system results in an efficient cross-current gas exchange system at the air capillary level (35). A remarkably thin blood-gas barrier is formed through attenuation of the epithelium (37), which entails complex processes of cell cutting and cell pinching (40). These mechanisms entail progressive loss of the apical parts of the epithelial cells (39, 40, 47). Fusion of the air space basement membrane with capillary endothelium basement membrane further contributes to reduction in blood-gas barrier thickness (10).

In the chicken embryo, the initial vessels encountered in the early lung bud were few and emanated from the central circulation. These vessels then increased in girth a few hours later and showed remarkable variation in girth, probably as a result of anastomoses with vasculogenic sinusoids (see Figs. 1 and 2). This network expanded initially by both sprouting and limited intussusception, but the latter process was supplanted by SA, which was the predominant mode of vascular formation during most of the early embryonic lung development.

Much is known about signaling events associated with angiogenesis, starting with a sprout; less is known of how an intact microvascular network is correctly formed following the initiation of sprouting (29). In the avian lung, the parabronchi are already well established by the time the smaller parabronchial vessels inaugurate, and these presumably form a guide to the developing blood vessels (see Figs. 2 and 3). Subsequently, the vasculature is formed to entirely engulf the parabronchus. Interestingly, rami of pulmonary artery and vein approach the parabronchi in step and at the same time and form a capillary network initially by sprouting. The rami form the interparabronchial arteries, which form the various subsequent generations described above.

Although vasculogenesis has been shown to be an important player of vascular development in the avian lung (5), little is known about how the elaborate vascular networks around the parabronchi are accomplished. Clearly, the current study underpins the fact that both sprouting and IA act contemporaneously in building the vascular network, albeit with differences in spatiotemporal distribution. Plausibly, the pulmonary vas-

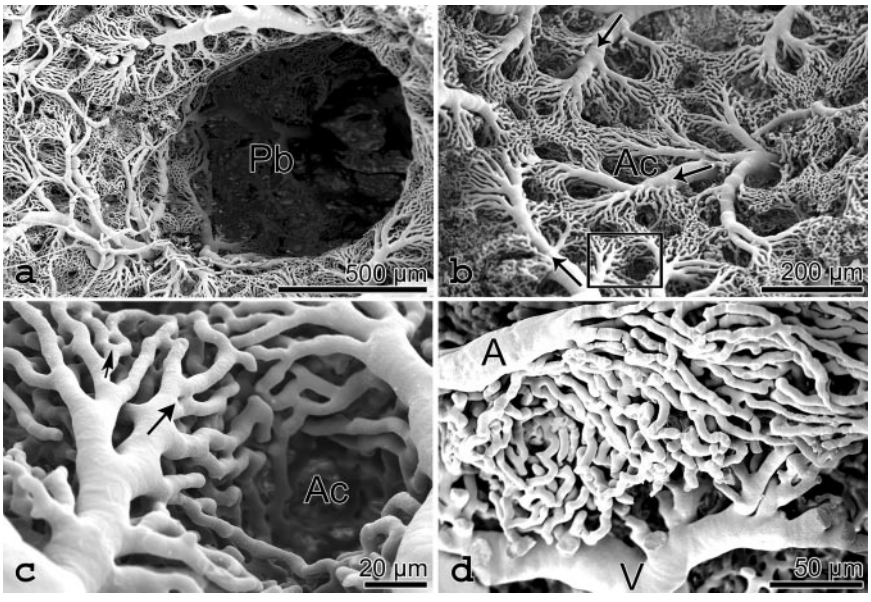

Fig. 6. Vascular corrosion casts showing the internal view of the parabronchial vasculature in the adult chicken. *A* and *B*: the internal aspect of the parabronchial vasculature is represented by hierarchically arranged draining veins (arrows) connected to the capillary plexus. Empty spaces represent air capillaries (Ac), and Pb is the parabronchial lumen. *C* and *D*: at a higher magnification, the rather elaborate pattern of the blood capillaries becomes evident. Note that the general direction of the capillaries is orthogonal to the long axis of the air capillaries (Ac), thus establishing a cross-current system at this level. Intussusceptive arborization remodels capillaries so that in the mature lung, slender and tubular blood capillaries course directly from the arterioles (A) and form a dense network around air capillaries and then drain into the venules. Pillars are occasionally encountered (arrows in *C*) and as a rule at the branching points. *C* is an *inset* of *B* (see rectangle in *B*).

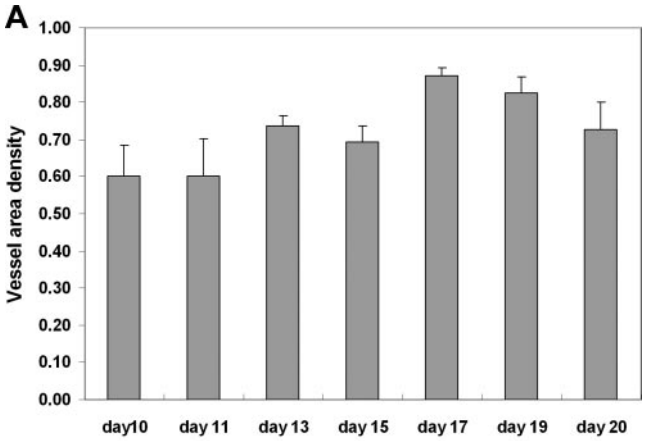

	day10	day 11	day 13	day 15	day 17	day 19	day 20
■ Relative numerical pillar density	11	17	24	42	118	285	453
□ Relative numerical sprout density	181	228	251	1475	931	380	178

Fig. 7. Bar graphs show mophometric measurements of the intussusceptive and sprouting angiogenesis in the lung of the developing chicken embryo. *A*: the vessel area density increases steadily reaching a peak at E17 as a result of both sprouting and intussusceptive angiogenesis. The progressive decrease in vessel density after E17 is a result of enlargement of tissue pillars that form bulky intervascular tissue meshes as well as reduction of sizes of vessels that form slender capillaries. *B*: assessment of the relative numerical densities of sprouts (i.e., number of sprouts/vessel area) and pillars (i.e., number of pillars/vessel area) demonstrating the interplay between both angiogenic modes in the various phases of development. Sprouting is predominant early during embryogenesis, with a dramatic peak at E15 and steady declines towards E20, whereas intussusception appears negligible in the early embryonic days but is preponderant from E17, with a peak before hatching.

culature inaugurates from vasculogenesis and SA, and while IA expands the initial primitive plexus, sprouting and migration form the plexuses surrounding the parabronchi. Vascular development during embryogenesis has been studied in the chick chorioallantoic membrane (22) and the kidney (41), and in both cases, participation of both sprouting and IA has been documented. The latter two organs, however, are transitory or have components that are evanescent and may not be an exact model of angiogenesis during organogenesis. Vascular development during organogenesis establishes networks that satisfy the functional needs of the organ while structurally conforming to the three-dimensional architecture of the organ. Recently, we have shown that in the evanescent mesonephros, SA precedes IA, but later the two processes become contemporaneous, with IA finally supplanting sprouting (41). In the current study, it is clear that early in development, both IA and sprouting build the initial network, with SA acting much earlier to move the sprouting entities to the targeted destinations. Hence, SA is the main process in the initial three quarters of embryonic period, after which it is completely supervened by IA. The latter angiogenic mechanism is responsible, in addition, for the formation of the organ-specific angioarchitecture. Sprouting is expensive in terms of time and resources. A sprout needs 2–3 days to be connected to the neighboring vasculature and get perfused. In contrast, IA requires just a few hours and needs no cell proliferation. This is the reason why the sprouting phase is three times longer than the intussusceptive one and the numerical density estimated for SA is high but relatively low for IA. The latter estimates do not correlate with impact of either of the mechanisms on lung vessel formation. When both processes are quantified in terms of density per vessel area, it is clear that although they remain contemporaneous, SA precedes and exceeds IA up to E15, when the latter becomes robust and the former declines.

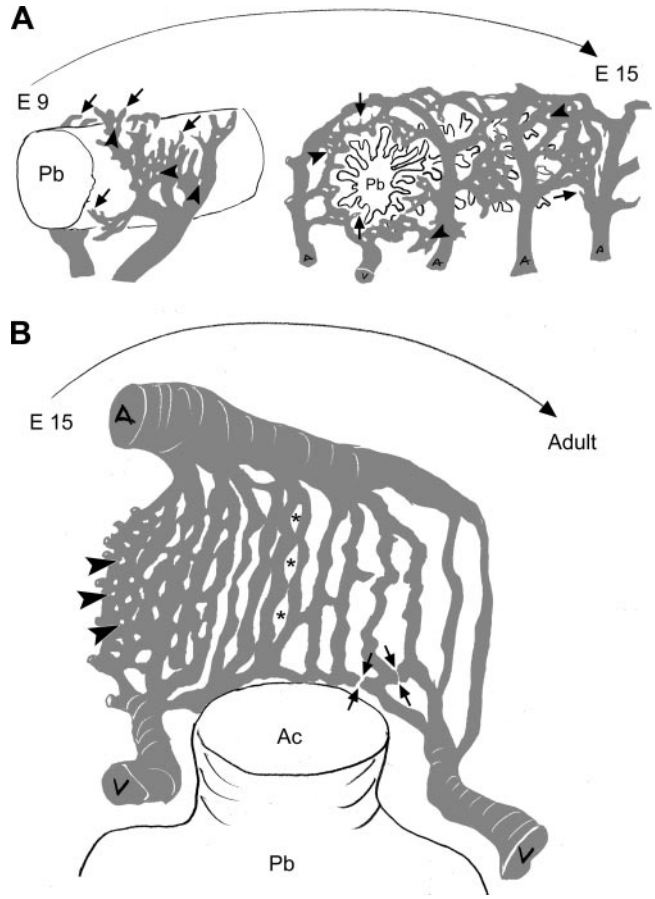

Fig. 8. Schematic illustration of vascular growth and remodeling during the formation of gas exchanging units. *A*: from E9 to E15 the capillary network expands by a wide front of sprouting vessels (arrows), followed by moderate intussusceptive pillar formation (arrowheads). Branches from parabronchial arteries approach the parabronchus (Pb) from both sides and form numerous sprouts that anastomose with each other. Note that at E9, the parabronchus is smooth, and no atria are formed at this stage. The parabronchial wall by E15 is invaded by several atrial outpouchings, which form infundibulae, and the first primitive air capillary sprouts. *B*: the segregation of the atrial microvasculature from E15 onward involves insertion of a multitude of tissue pillars (arrowheads). The pillars reshape and fuse successively (*) delineating straight solitary capillary segments around the air capillaries (Ac). Transversal vascular connections surrounding air capillary entrances are severed (double arrows), which shifts the blood into the slender and tubular blood capillaries from the arterioles (A) into the draining venules (V), forming in this way the final vascular pattern of the chicken lung.

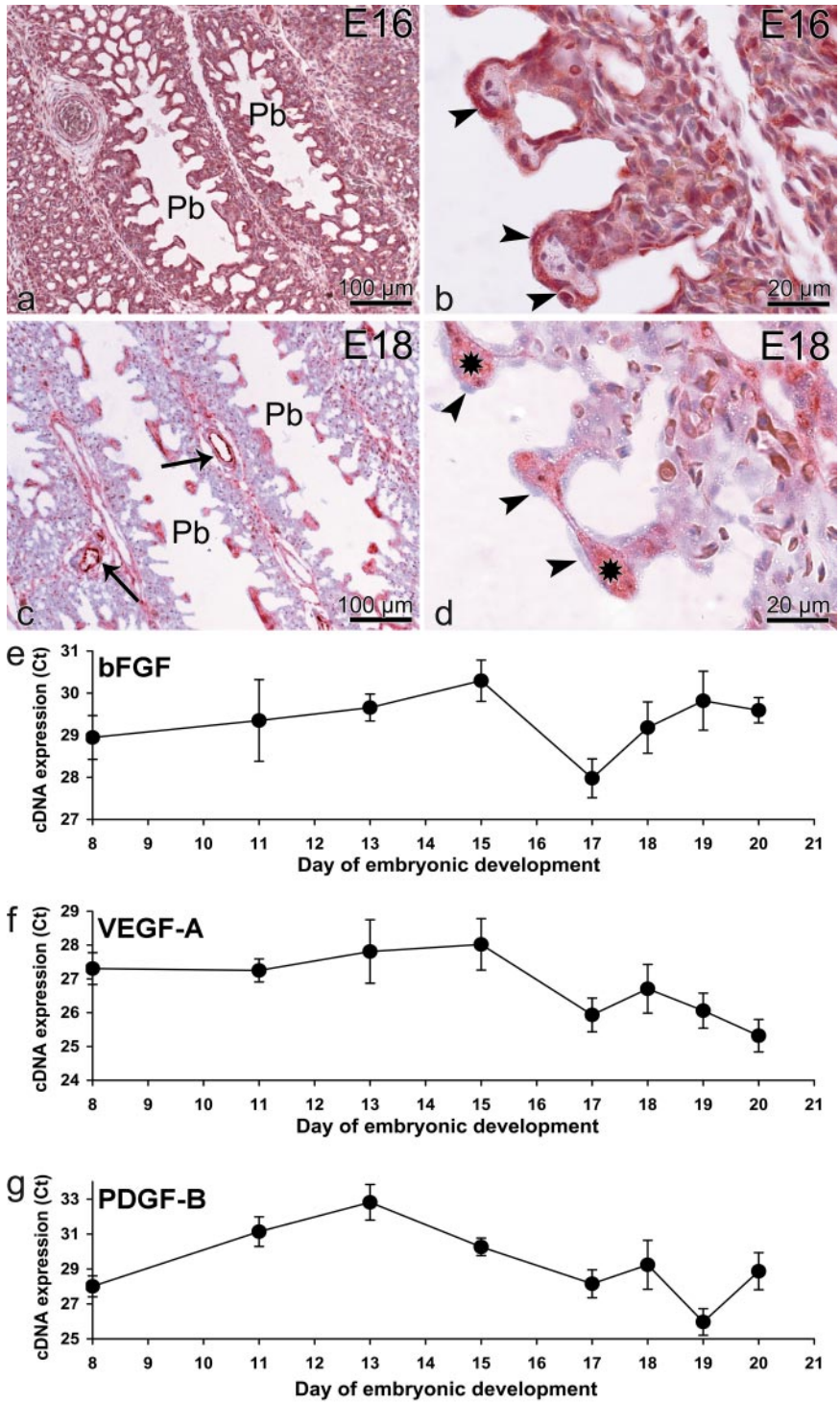

Fig. 9. Micrographs show immunoreactivity for VEGF and basic FGF (bFGF) and graphs demonstate alterations in the cDNA expression of bFGF, VEGF, and PDGF-B. *A–D*: VEGF (*A* and *B)* was strongly expressed in the lung epithelial cells (arrowheads in *B*) and sparsely in the stroma. On the contrary, bFGF (*C* and *D*) was diffusely expressed in the stromal compartment (*) and small feeding vessels (arrows), whereas the epithelium (arrowheads in *D*) remained negative. *B* is an *inset* of *A*, and *D* is an *inset* of *C*. Pb, parabronchi. *E–G*: the alteration in the cDNA expression was conspicuous in the last 6 days of incubation. Before E15, VEGF and bFGF were maintained at moderate and almost constant levels. The peak of bFGF and VEGF at E17 is followed by rise of VEGF and PDGF-B at E19. Notice the remarkable upsurge of PDGF-B on E19.

Inception, expansion, remodeling, and maturation of the developing vasculature are driven by a host of growth factors, genes, and physiological conditions, including hemodynamic forces (13, 51). VEGF is important for SA, fine patterning of growing vessel networks during embryogenesis and in postnatal life, and also controls several processes in endothelial cells, such as proliferation, survival, and migration (25, 25, 46). It modulates angiogenic sprouting in the early postnatal retina by guiding filopodial extensions from specialized endothelial cells situated at the tips of the vascular sprouts. The vessel patterning during retinal angiogenesis depends on VEGF-A distribution (27), and VEGF signaling is associated with assembly (6) as well as pattering of embryonic vasculature (4, 31). Probably similar to the retinal angiogenesis, expression of VEGF by the epithelial cells stimulates formation of endothelial sprouts, which approach the air spaces until the vascular and epithelial basal laminas merge, thus forming the thin blood-gas barrier.

The factors that drive lung angio- and morphogenesis are currently not very well understood. Generally, FGFs and FGF receptors are expressed in the developing lung and appear to be major regulators of lung growth and differentiation (12). bFGF is strongly expressed in the developing chicken embryo lung tissue (36), and in the quail embryo, it induces angioblasts and patterns blood vessel formation (15). However, the exact role of endogenous bFGF in angiogenesis remains uncertain. Indeed, bFGF knockout mice and transgenic mice overexpressing bFGF do not have significant morphological alterations and functional abnormalities (26, 45, 52).

Our earlier investigations demonstrated that the sprouting phase in the developing kidney is related to a high VEGF expression, whereas IA is associated with a preponderance of bFGF (41). Recently, investigations have demonstrated that VEGF and bFGF act together. It has been shown that bFGF induces neovascularization indirectly by activation of the VEGF/VEGFR system, inducing angiogenesis in different ways, and also activates motility factors for pericytes, therefore influencing vascular remodeling and maturation (28, 42, 44, 48).

Together, we could speculate that that VEGF and bFGF act in synergy; in a first step, VEGF induces multiple capillary sprouts that invade the mesenchyme and form the primitive capillary plexus. Further vascular growth and remodeling occurs by intussusception, probably supported by bFGF. Data furnished by Tomanek et al. (48a) supported the VEGF/bFGF "two-step" hypothesis, which showed that vascular tube formation, initially induced by VEGF, is totally abolished by neutralizing antibodies to bFGF. PDGF-B is essential for pericyte recruitment (7, 9) and therefore may be important in formation and maturation of the tissue pillars during IA (20, 21). The remarkable upsurge of PDGF-B observed at E19 in this study probably indicates a narrow window when robust pericyte recruitment takes place.

In addition to regulatory molecules, circulatory flow dynamics play an important role in helping to determine the pattern of interconnections between the primary network and secondary sprouts, and thus the final arterial or venous identity of the vessels in the functional network (23, 32). It seems that blood flow acts on genetically predetermined vascular plexus (13). Flow shapes the global patterning of the arterial tree and regulates the activation of the arterial markers such as ephrin B2 and neuropilin-1 (33). Embryonic cardiovascular adaptation to changes in metabolic and hemodynamic demands occurs at the tissue and cellular levels; however, there are limits to adaptation that result in a normal mature phenotype (25).

In the chicken lung, establishment of the vascular network relies largely on capillary migration and transdifferentiation into arterioles and arteries as well as anastomoses, perhaps guided by ehprins and ephrin receptors, which are known to integrate blood vessel and tissue morphogenesis (1). Eph signaling is requisite for SA and blood vessel remodeling during vascular development (14). In addition to flow dynamics, genetic programs control arterial-venous cell fate and blood vessel identity (2).

In conclusion, we note that the vasculature of the avian lung inaugurates through the processes of vasculogenesis and angiogenesis. The formation of the basic pattern is accomplished by sprouting, whereas expansion of the vascular patterns, refinement of the finer vascular entities, and formation of the final vascular phenotype typical for the avian lung is by intussusception. These processes are probably supported by interplay between several angiogenic factors with both VEGF and bFGF playing a major role.

ACKNOWLEDGMENTS

We thank Karl Babl, Christoph Lehmann, Beat Haenni, J. M. Gachoka, Krystyna Sala, Bettina de Breuyn, Barbara Krieger, and Amos Tangai for excellent technical assistance and Dr. H. R. Duncker for helpful discussions. Grace Ndegwa kindly provided the adult hens on which part of this work is based.

GRANTS

We acknowledge financial support from the Swiss National Science Foundation through Grants 31-45831.95, 31-55895.98, and 31-55895.98/2 and the Bernese Cancer League.

REFERENCES

1. **Adams RH.** Vascular patterning by Eph receptor tyrosine kinases and ephrins. *Semin Cell Dev Biol* 13: 55–60, 2002.
2. **Adams RH.** Molecular control of arterial-venous blood vessel identity. *J Anat* 202: 105–112, 2003.
3. **Ambler CA, Nowicki JL, Burke AC, Bautch VL.** Assembly of trunk and limb blood vessels involves extensive migration and vasculogenesis of somite-derived angioblasts. *Dev Biol* 234: 352–364, 2001.
4. **Ambler CA, Schmunk GM, Bautch VL.** Stem cell-derived endothelial cells/progenitors migrate and pattern in the embryo using the VEGF signaling pathway. *Dev Biol* 257: 205–219, 2003.
5. **Anderson-Berry A, O'Brien EA, Bleyl SB, Lawson A, Gundersen N, Ryssman D, Sweeley J, Dahl MJ, Drake CJ, Schoenwolf GC, Albertine KH.** Vasculogenesis drives pulmonary vascular growth in the developing chick embryo. *Dev Dyn* 233: 145–153, 2005.
6. **Argraves WS, Larue AC, Fleming PA, Drake CJ.** VEGF signaling is required for the assembly but not the maintenance of embryonic blood vessels. *Dev Dyn* 225: 298–304, 2002.
7. **Armulik A, Abramsson A, Betsholtz C.** Endothelial/pericyte interactions. *Circ Res* 97: 512–523, 2005.
8. **Bellairs R, Osmond M.** *The Atlas of Chick Development*. London: Academic, 1998.
9. **Betsholtz C, Lindblom P, Gerhardt H.** Role of pericytes in vascular morphogenesis. *EXS* 94: 115–125, 2005.
10. **Brody JS, Williams MC.** Pulmonary alveolar epithelial cell differentiation. *Annu Rev Physiol* 54: 351–371, 1992.
11. **Burri PH, Hlushchuk R, Djonov V.** Intussusceptive angiogenesis: its emergence, its characteristics, and its significance. *Dev Dyn* 231: 474–488, 2004.
12. **Cardoso WV, Itoh A, Nogawa H, Mason I, Brody JS.** FGF-1 and FGF-7 induce distinct patterns of growth and differentiation in embryonic lung epithelium. *Dev Dyn* 208: 398–405, 1997.
13. **Carmeliet P.** Angiogenesis in life, disease and medicine. *Nature* 438: 932–936, 2005.
14. **Cheng N, Brantley DM, Chen J.** The ephrins and Eph receptors in angiogenesis. *Cytokine Growth Factor Rev* 13: 75–85, 2002.
15. **Cox CM, Poole TJ.** Angioblast differentiation is influenced by the local environment: FGF-2 induces angioblasts and patterns vessel formation in the quail embryo. *Dev Dyn* 218: 371–382, 2000.
16. **De La RR.** Photonic crystals: microassembly in 3D. *Nat Mater* 2: 74–76, 2003.
17. **deMello DE, Reid LM.** Embryonic and early fetal development of human lung vasculature and its functional implications. *Pediatr Dev Pathol* 3: 439–449, 2000.
18. **deMello DE, Sawyer D, Galvin N, Reid LM.** Early fetal development of lung vasculature. *Am J Respir Cell Mol Biol* 16: 568–581, 1997.
19. **DeRuiter MC, Gittenberger-de Groot AC, Poelmann RE, VanIperen L, Mentink MM.** Development of the pharyngeal arch system related to the pulmonary and bronchial vessels in the avian embryo. With a concept on systemic-pulmonary collateral artery formation. *Circulation* 87: 1306–1319, 1993.
20. **Djonov V, Baum O, Burri PH.** Vascular remodeling by intussusceptive angiogenesis. *Cell Tissue Res* 314: 107–117, 2003.
21. **Djonov V, Makanya AN.** New insights into intussusceptive angiogenesis. *EXS* 94: 17–33, 2005.

22. **Djonov VG, Kurz H, Burri PH.** Optimality in the developing vascular system: branching remodeling by means of intussusception as an efficient adaptation mechanism. *Dev Dyn* 224: 391–402, 2002.
23. **Dor Y, Djonov V, Keshet E.** Making vascular networks in the adult: branching morphogenesis without a roadmap. *Trends Cell Biol* 13: 131–136, 2003.
24. **Drake CJ.** Embryonic and adult vasculogenesis. *Birth Defects Res C Embryo Today* 69: 73–82, 2003.
25. **Ferrara N, Kerbel RS.** Angiogenesis as a therapeutic target. *Nature* 438: 967–974, 2005.
26. **Fulgham DL, Widhalm SR, Martin S, Coffin JD.** FGF-2 dependent angiogenesis is a latent phenotype in basic fibroblast growth factor transgenic mice. *Endothelium* 6: 185–195, 1999.
27. **Gerhardt H, Golding M, Fruttiger M, Ruhrberg C, Lundkvist A, Abramsson A, Jeltsch M, Mitchell C, Alitalo K, Shima D, Betsholtz C.** VEGF guides angiogenic sprouting utilizing endothelial tip cell filopodia. *J Cell Biol* 161: 1163–1177, 2003.

27a. **Gundersen HJG.** Notes on the estimation of the numerical density of arbitary profiles: the edge effect. *J Microsc* 111: 219–223, 1977.

28. **Hagedorn M, Balke M, Schmidt A, Bloch W, Kurz H, Javerzat S, Rousseau B, Wilting J, Bikfalvi A.** VEGF coordinates interaction of pericytes and endothelial cells during vasculogenesis and experimental angiogenesis. *Dev Dyn* 230: 23–33, 2004.
29. **Hansen-Smith FM.** Capillary network patterning during angiogenesis. *Clin Exp Pharmacol Physiol* 27: 830–835, 2000.
30. **Hislop A.** Developmental biology of the pulmonary circulation. *Paediatr Respir Rev* 6: 35–43, 2005.
31. **Hogan KA, Ambler CA, Chapman DL, Bautch VL.** The neural tube patterns vessels developmentally using the VEGF signaling pathway. *Development* 131: 1503–1513, 2004.
32. **Isogai S, Lawson ND, Torrealday S, Horiguchi M, Weinstein BM.** Angiogenic network formation in the developing vertebrate trunk. *Development* 130: 5281–5290, 2003.
33. **Le Noble F, Moyon D, Pardanaud L, Yuan L, Djonov V, Matthijsen R, Breant C, Fleury V, Eichmann A.** Flow regulates arterial-venous differentiation in the chick embryo yolk sac. *Development* 131: 361–375, 2004.
34. **Maina JN.** Scanning electron microscope study of the spatial organization of the air and blood conducting components of the avian lung (*Gallus gallus variant domesticus*). *Anat Rec* 222: 145–153, 1988.
35. **Maina JN.** Is the sheet-flow design a 'frozen core' (a Bauplan) of the gas exchangers? Comparative functional morphology of the respiratory microvascular systems: illustration of the geometry and rationalization of the fractal properties. *Comp Biochem Physiol A Mol Integr Physiol* 126: 491–515, 2000.
36. **Maina JN.** A systematic study of the development of the airway (bronchial) system of the avian lung from days 3 to 26 of embryogenesis: a transmission electron microscopic study on the domestic fowl, *Gallus gallus variant domesticus*. *Tissue Cell* 35: 375–391, 2003.
37. **Maina JN.** Developmental dynamics of the bronchial (airway) and air sac systems of the avian respiratory system from day 3 to day 26 of life: a scanning electron microscopic study of the domestic fowl, *Gallus gallus variant domesticus*. *Anat Embryol* 207: 119–134, 2003.
38. **Maina JN.** Morphogenesis of the laminated, tripartite cytoarchitectural design of the blood-gas barrier of the avian lung: a systematic electron microscopic study on the domestic fowl, *Gallus gallus variant domesticus*. *Tissue Cell* 36: 129–139, 2004.
39. **Maina JN.** Systematic analysis of hematopoietic, vasculogenetic, and angiogenetic phases in the developing embryonic avian lung, *Gallus gallus variant domesticus*. *Tissue Cell* 36: 307–322, 2004.
40. **Makanya AN, Hlushchuk R, Duncker HR, Draeger A, Djonov V.** Epithelial transformations in the establishment of the blood-gas barrier in the developing chick embryo lung. *Dev Dyn* 235: 68–81, 2006.
41. **Makanya AN, Stauffer D, Ribatti D, Burri PH, Djonov V.** Microvascular growth, development, and remodeling in the embryonic avian kidney: the interplay between sprouting and intussusceptive angiogenic mechanisms. *Microsc Res Tech* 66: 275–288, 2005.
42. **Nico B, Mangieri D, Corsi P, De Giorgis M, Vacca A, Roncali L, Ribatti D.** Vascular endothelial growth factor-A, vascular endothelial growth factor receptor-2 and angiopoietin-2 expression in the mouse choroid plexuses. *Brain Res* 1013: 256–259, 2004.
43. **Noden DM.** Origins and assembly of avian embryonic blood vessels. *Ann NY Acad Sci* 588: 236–249, 1990.
44. **Presta M, Dell'Era P, Mitola S, Moroni E, Ronca R, Rusnati M.** Fibroblast growth factor/fibroblast growth factor receptor system in angiogenesis. *Cytokine Growth Factor Rev* 16: 159–178, 2005.
45. **Ribatti D, Nico B, Morbidelli L, Donnini S, Ziche M, Vacca A, Roncali L, Presta M.** Cell-mediated delivery of fibroblast growth factor-2 and vascular endothelial growth factor onto the chick chorioallantoic membrane: endothelial fenestration and angiogenesis. *J Vasc Res* 38: 389–397, 2001.
46. **Ruhrberg C.** Growing and shaping the vascular tree: multiple roles for VEGF. *Bioessays* 25: 1052–1060, 2003.
47. **Scheuermann DW, Klika E, Groodt-Lasseel MH, Bazantova I, Switka A.** The development and differentiation of the parabronchial unit in quail (*Coturnix coturnix*). *Eur J Morphol* 36: 201–215, 1998.
48. **Tille JC, Wood J, Mandriota SJ, Schnell C, Ferrari S, Mestan J, Zhu Z, Witte L, Pepper MS.** Vascular endothelial growth factor (VEGF) receptor-2 antagonists inhibit VEGF- and basic fibroblast growth factor-induced angiogenesis in vivo and in vitro. *J Pharmacol Exp Ther* 299: 1073–1085, 2001.

48a. **Tomanek RJ, Sandra A, Zheng W, Brock T, Bjercke RJ, Holifield JS.** Vascular endothelial growth factor and basic fibroblast growth factor differentially modulate early postnatal coronary angiogenesis. *Cir Res* 88: 1135–1141, 2001.

49. **Vu TH, Alemayehu Y, Werb Z.** New insights into saccular development and vascular formation in lung allografts under the renal capsule. *Mech Dev* 120: 305–313, 2003.
50. **West NH, Bamford OS, Jones DR.** A scanning electron microscope study of the microvasculature of the avian lung. *Cell Tissue Res* 176: 553–564, 1977.
51. **Wilting J, Christ B, Yuan L, Eichmann A.** Cellular and molecular mechanisms of embryonic haemangiogenesis and lymphangiogenesis. *Naturwissenschaften* 90: 433–448, 2003.
52. **Zhou M, Sutliff RL, Paul RJ, Lorenz JN, Hoying JB, Haudenschild CC, Yin M, Coffin JD, Kong L, Kranias EG, Luo W, Boivin GP, Duffy JJ, Pawlowski SA, Doetschman T.** Fibroblast growth factor 2 control of vascular tone. *Nat Med* 4: 201–207, 1998.